Inorganica Chimica Acta, 133 (1987) 167–173

Photophysics of Ce^{3+} Cryptates

G. BLASSE, G. J. DIRKSEN

Physical Laboratory, Utrecht University, P.O.B. 80.000, 3508 TA Utrecht, The Netherlands

N. SABBATINI and S. PERATHONER

Dipartimento di Chimica 'G. Ciamician' dell'Universitá, 40 126 Bologna, Italy

(Received February 18, 1987)

Abstract

The species $[Ce^{3+} \subset 2.2.1]$ and $[Ce^{3+} \subset 2.2.2]$ show efficient ultraviolet luminescence at room temperature. The spectra have been analysed and are discussed. The Stokes shift of the emission is smaller in the solid state than in solution. This is discussed in connection with the configuration of the species. In solid $[Ce^{3+} \subset 2.2.1]Cl_3 \cdot 2H_2O$ energy transfer between the cryptate species leads to a diffusion length of about 60 Å. A comparison with the related Eu^{2+} cryptates is made. The crystal-field splitting of the excited 5d level is derived and compared for these cryptates and some crown-ether complexes.

Introduction

Certain diazapolyoxabicyclic ligands (cryptands) [1] can form stable complexes with metal ions. The photophysical properties of some of these complexes have been reported recently, using the 4,7,13,16,21,24-hexaoxa-1,10-diazabicyclo[8.8.8]-hexacosane (called [2.2.2]) and 4,7,13,16,21-pentaoxa-1,10-diaza-bicyclo[8.8.5]tricosane (called [2.2.1]) cryptands. Figure 1 shows a schematic representation of these cryptands.

The $[Eu^{2+} \subset 2.2.1]$ and $[Eu^{2+} \subset 2.2.2]$ cryptates show efficient luminescence below room temperature [2]. The $[Eu^{3+} \subset 2.2.1]$ cryptate has a much lower efficiency of its luminescence because of the predominance of non-radiative transitions due to the presence of a low-lying charge-transfer state and high frequency vibrations in the surroundings (H_2O) [3, 4]. In $[Sm^{3+} \subset 2.2.1]$ cryptate the non-radiative transitions dominate also; here they are due to high frequency vibrations only [5]. In $[Tb^{3+} \subset 2.2.1]$ their influence can be reduced considerably and a quantum efficiency of 0.3 results [5]. This is even more true for $[Gd^{3+} \subset 2.2.1]$, where the efficiency is 1 [6].

In this paper we report on the photophysical properties of Ce^{3+} cryptates. The Ce^{3+} ion with a $4f^1$ configuration shows allowed optical transitions in absorption and emission which are of the $f \rightarrow d$ type [7]. The $[Ce^{3+} \subset 2.2.1]$ and $[Ce^{3+} \subset 2.2.2]$ cryptates show efficient luminescence in the ultraviolet spectral region, in solution as well as in the solid state. This study reveals energy transfer between $[Ce^{3+}$ 2.2.1] ions in the solid state at room temperature. This is a surprising result, since the cryptand ligand keeps the Ce^{3+} ions far apart (~10 Å).

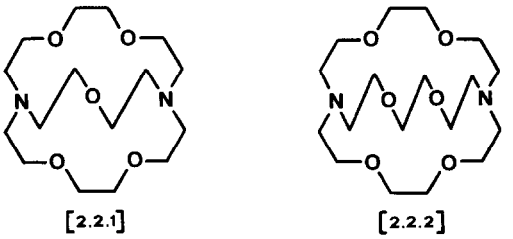

Fig. 1. The [2.2.1] and [2.2.2] cryptands.

The spectroscopic results are also used to speculate about the configuration of the cryptate, which appears to depend critically on the ionic radius of the metal ion. The results for Ce^{3+} are compared with those for the Eu^{2+} cryptates, because the Eu^{2+} ion also shows $f \rightarrow d$ transitions in its spectra. Finally, the crystal-field splitting of the excited d level is discussed.

Experimental

The $[Ce^{3+} \subset 2.2.1]$ and $[Ce^{3+} \subset 2.2.2]$ cryptates were prepared following the same procedure as described in refs. 3 and 5 for the analogous Eu^{3+}, Sm^{3+} and Tb^{3+} compounds. Purified samples were obtained by recrystallization from methanol. The Eu^{3+}-doped Ce^{3+} cryptate was obtained from Eu^{3+} cryptate and Ce^{3+} cryptate by dissolving the cryptates in the required proportions.

The photophysical measurements were performed as described in previous papers [2–6].

0020-1693/87/$3.50

Results

In solution as well as in the solid state the [$Ce^{3+} \subset$ 2.2.1] and [$Ce^{3+} \subset$ 2.2.2] cryptates show efficient luminescence in the ultraviolet region. The quantum efficiencies at room temperature and below are 1, with the exception of the unpurified solid [$Ce^{3+} \subset$ 2.2.1] samples (see below). Figure 2 shows some of the emission and excitation spectra of the luminescence of [$Ce^{3+} \subset$ 2.2.1], whereas Fig. 3 gives the

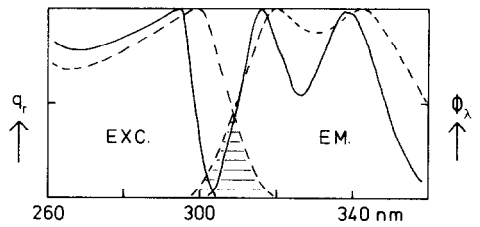

Fig. 2. Emission (EM) and excitation (EXC) spectra of the luminescence of solid [$Ce^{3+} \subset$ 2.2.1]$Cl_3 \cdot 2H_2O$ at 4.2 K (drawn lines) and 300 K (broken lines). The spectral overlap of emission and excitation spectra at 300 K has been hatched. The excitation wavelength is 290 nm and the emission wavelength monitored is 340 nm. q_r gives the relative quantum output, and ϕ_λ the spectral radiant power per constant wavelength interval, both in arbitrary units.

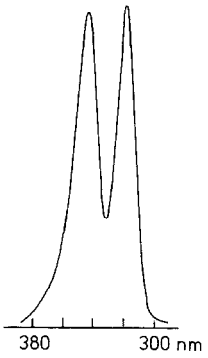

Fig. 3. The emission spectrum of solid [$Ce^{3+} \subset$ 2.2.2]$Cl_3 \cdot 2H_2O$ at 4.2 K. Excitation wavelength is 285 nm. Notation as in Fig. 2.

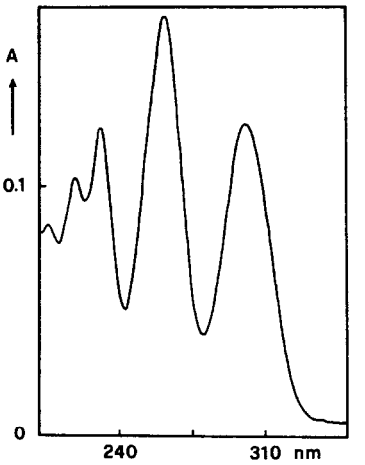

Fig. 4. The absorption spectrum of a solution of [$Ce^{3+} \subset$ 2.2.1] in water (3.6×10^{-4} M). A is the absorbance.

low temperature emission spectrum of [$Ce^{3+} \subset$ 2.2.2]. Figure 4 presents the absorption spectrum of [$Ce^{3+} \subset$ 2.2.1] in solution. In Table I several luminescence characteristics have been collected. Note that the spectra for the species in solution and for those in the solid state are different. The excitation spectra correspond to the absorption spectra, however, the latter could be measured up to shorter wavelengths than the former. Those for the solid samples do not give much information due to the high absorption strength of these samples.

The emission spectra of the solid samples show a considerable broadening when the temperature is increased from 4.2 to 300 K. This broadening was fitted to the formula

$$\sigma(T) = \sigma(0)\left[\tan h \frac{h\nu_e}{2kT}\right]^{-1/2} \qquad [8]$$

Here σ presents the half-width of a single emission band and ν_e the frequency of an effective vibrational mode which is responsible for the broadening. We

TABLE I. Some Photophysical Properties of Ce^{3+} Cryptates under Different Conditions

Sample	T (K)	Emission maxima (nm)	Excitation maxima (nm)	Stokes shift (10^3 cm^{-1})	Decay time (ns)
[$Ce^{3+} \subset$ 2.2.1] solid	4.2	338, 316	295, ~260	2.3	
	300	342, 320	300, ~260	2.1	30
[$Ce^{3+} \subset$ 2.2.1] solution	300	360, 340	300, 258	3.9	50[a]
[$Ce^{3+} \subset$ 2.2.2] solid	4.2	345, 319	283, ~255	4.0	
	300	345, 317	287, ~260	3.3	
[$Ce^{3+} \subset$ 2.2.2] solution	300	~370[b], 352	270, 252	8.6	50

[a]30 ns at 77 K. [b]Shoulder.

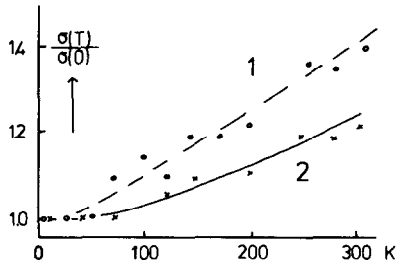

Fig. 5. Temperature dependence of the relative emission band width of the luminescences of solid [$Ce^{3+} \subset$ 2.2.1] (circles) and of solid [$Ce^{3+} \subset$ 2.2.2] (crosses). The drawn and the broken curves represent fit curves, as discussed in the text. $\sigma(T)$ indicates the band width of the individual components of the emission band at the temperature T.

find for [$Ce^{3+} \subset$ 2.2.1] $\nu_e \simeq 150$ cm^{-1} and for [$Ce^{3+} \subset$ 2.2.2] $\nu_e \simeq 300$ cm^{-1} (Fig. 5).

Table I also contains several values for the luminescence decay time.

The luminescence intensity of the unpurified solid [$Ce^{3+} \subset$ 2.2.1] sample shows a decrease as a function of increasing temperature above ~250 K. As a consequence, the room temperature intensity is 2/3 of that at low temperatures. However, after purification this decrease is no longer observed. If the purified sample is contaminated with 1% Eu^{3+} cryptate, a similar decrease occurs. The Eu^{3+} emission is observed only for excitation into the $4f^6$ levels ($^5L_6$ and lower), not for excitation into the Ce^{3+} cryptate. For [$Ce^{3+} \subset$ 2.2.2] this temperature effect was not observed.

According to measurements on the solid samples, there is always a second phase present, more in the original than in the purified samples. This second phase shows a typical Ce^{3+} emission band with emission maxima at 390 and 360 nm. The corresponding excitation maxima are 332 and 310 nm (values at 4.2 K). These spectra are identical for both cryptates. Neither the spectral positions nor the intensities of these features change upon heating to room temperature. We did not observe any energy transfer from the cryptate to the second phase, which obviously does not interfere with the photophysical phenomena in the Ce^{3+} cryptate. The nature of the second phase is hard to unravel, but it seems probable that it is a cerium chloride (hydrated) or a cerium oxychloride. Compounds of this type show emission in the same spectral region as the second phase [7, 9].

Discussion

The Luminescence Spectra of the Ce^{3+} Cryptates

The energy level scheme of the Ce^{3+} ion is rather simple. The ground state configuration ($4f^1$) yields two levels, *viz.* $^2F_{5/2}$ and $^2F_{7/2}$; the excited state configuration ($5d^1$) yields a couple of crystal-field split components, the total splitting being of the order of 10 000 cm^{-1} [7]. The transitions between the $4f^1$ and $5d^1$ configurations are completely allowed as electric dipole transitions. This explains immediately the very short (radiative) decay times.

All emission spectra consist of a double band with maxima separated by some 2000 cm^{-1}. This corresponds to the ground-state splitting ($^2F_{5/2}$–$^2F_{7/2}$). The absorption spectra (Fig. 4) show five components, reflecting the low site symmetry for Ce^{3+} in the cryptates. The centre of gravity of the 5d level is 41 900 cm^{-1} for [$Ce^{3+} \subset$ 2.2.1] and 42 650 cm^{-1} for [$Ce^{3+} \subset$ 2.2.2]. These values are nearly 10 000 cm^{-1} higher than for Ce^{3+} in non-molecular solid oxides [7] and tend to approach the values observed for fluorides (44 000 cm^{-1} for Ce^{3+} in CaF_2 [10] and 48 000 cm^{-1} for Ce^{3+} in SrF_2 [11]). This implies that the bonding of the cryptates to the Ce^{3+} ion is only weakly covalent.

Let us now consider the Stokes shift of the emission. For Ce^{3+} in aqueous solution, the Stokes shift is some 5000 cm^{-1} [12]. For Ce^{3+} in non-molecular solids, much smaller as well as similar values have been reported [7]: $ScBO_3$–Ce, 1200 cm^{-1}; $YAl_3B_4O_{12}$–Ce, 1900 cm^{-1}; YOCl–Ce, 5300 cm^{-1}, for example. The small values correspond to Ce^{3+} in six-coordination. With these figures in mind it is clear that the Stokes shift of [$Ce^{3+} \subset$ 2.2.1] in the solid state (see Table I) is remarkably small. This implies that the relaxation in the excited state is strongly restricted. It is striking that the [2.2.1] cryptand forms such a firm surrounding around the Ce^{3+} ion that it can be compared to those non-molecular host lattices where the Ce^{3+} ion occupies a site which offers a very small amount of space. This strongly suggests that the Ce^{3+} ion occupies the centre of the cryptand in solid [$Ce^{3+} \subset$ 2.2.1]. Actually, the ionic radius of the Ce^{3+} ion (1.14 Å [13]) is equal to the radius of the [2.2.1] cavity (1.1 Å [2]).

In this connection it is interesting to note that the effective vibrational frequency which is responsible for the emission band broadening amounts to 150 cm^{-1}. This value is too low to correspond to Ce^{3+}–O(N) stretching or bending modes. It may well be that this frequency corresponds to a mode in which the whole cryptand moves relative to the Ce^{3+} ion. A similar frequency was observed in the vibronic emission lines of the Eu^{3+} ion in [$Eu^{3+} \subset$ 2.2.1] [4].

The radius of the [2.2.2] cavity (1.4 Å [2]) is considerably larger. It seems even probable that the Ce^{3+} ion is off-centre in this cryptand. This offers a better possibility for relaxation in the excited state than the [2.2.1] cryptand. Actually the Stokes shift in the case of solid [$Ce^{3+} \subset$ 2.2.2] is much larger

(see Table I). The effective frequency ν_e is higher, *viz.* 300 cm^{-1}; this value corresponds to Ce^{3+}–O(N) bending. This also shows that the Ce^{3+} ion in the [2.2.2] cryptand is bonded differently from that in the [2.2.1] cryptand.

In solution the Stokes shift is much larger than in the solid state (see Table I). In the case of [Ce^{3+} ⊂ 2.2.1] the absorption (excitation) spectra are equal in solution and in the solid state. The difference in Stokes shift corresponds, therefore, to a difference in relaxation after excitation. This is rather obvious and was also observed for the charge-transfer state of [Eu^{3+} ⊂ 2.2.1] [4]. In the case of [Ce^{3+} ⊂ 2.2.2] even the absorption (excitation) spectra are different for solution and solid state (see Table I), suggesting that even in the ground state the Ce^{3+} ion occupies the [2.2.2] cavity in the solid in a different way from in solution.

Energy Transfer in Solid [Ce^{3+} ⊂ 2.2.1]Cl_3

Figure 2 shows that at room temperature there is a considerable spectral overlap between the emission and absorption (excitation) spectra of [Ce^{3+} ⊂ 2.2.1]. This is due to the small Stokes shift on one hand and to the considerable thermal broadening of the spectral bands on the other. This overlap suggests that energy transfer from one cryptate molecule to another is feasible. Since all optical transitions involved are allowed electric dipole, it is easy to calculate the critical transfer distance R_c. We used the following data: spectral overlap $SO = 0.3$ eV^{-1} (from our spectra), oscillator strength of the Ce^{3+} absorption transition $P = 10^{-2}$ [14], energy of maximum spectral overlap $E = 4$ eV (from our spectra). Introducing these in the equation [15, 16]

$$R_c^6 = 0.6 \times 10^{28} \frac{4.8 \times 10^{-16} P}{E^4} SO$$

yields 18 Å for R_c (300 K). At 4.2 K the term SO has decreased dramatically ($SO = 5 \times 10^{-5}$ eV^{-1}), and R_c (4.2 K) is only 4 Å.

The Ce^{3+}–Ce^{3+} distance is about 10 Å [4, 17] so that at low temperatures energy transfer is impossible. However, at 300 K the transfer probability exceeds the radiative rate by a factor of $(18/10)^6 = 34$. Energy transfer between the cryptate species will, therefore, take place.

Whether this phenomenon will result in quenching of the luminescence, depends on whether the diffusion length of the excited state is long enough to reach the quenching sites. The diffusion length is equal to $10\sqrt{34}$ Å ≃ 60 Å (the shortest Ce^{3+}–Ce^{3+} distance is 10 Å), so that the excited state covers a sphere of $\frac{4}{3}\pi 60^3$ $Å^3$ ≃ 9×10^5 $Å^3$. Since at 300 K 1/3 of the low-temperature emission of the unpurified sample is quenched, there must be at least 1 quenching site per 3×10^6 $Å^3$. One ion [Ce^{3+} ⊂ 2.2.1] occupies some 1000 $Å^3$, taking into account its radius, the counter ions and water molecules, and empty space. This means that the quenching site concentration is at least 1 quencher per 3000 cryptate molecules, *viz.* 0.03%.

The only (very rough) possibility we have to check this value is the diffuse reflection spectrum. This shows, next to the Ce^{3+} cryptate absorption bands, a tail into the longer wavelength area. If we use this in order to estimate with the Kubelka–Munk function [18] the concentration of the species responsible for the tail, we arrive at 0.2%. In view of the approximate character of this method, the agreement with the calculated 0.03% is reasonable. So the conclusion must be that the quenching of the luminescence intensity of the unpurified solid [Ce^{3+} ⊂ 2.2.1] near 300 K is due to thermally activated energy migration to quenching sites.

At 4.2 K the energy transfer does not occur. If transfer from [Ce^{3+} ⊂ 2.2.1] to quenching sites still takes place, its influence on the luminescence intensity is negligible: if the cryptate has twelve neighbours, the probability that among these twelve there is no quencher is $0.9997^{12} \simeq 0.996$, *i.e.* the quenching amounts to less than 1%.

The quenching will also not occur if the quenching site concentration is decreased. If, for example, this concentration decreases one order of magnitude, the amount of quenching at 300 K is only about 3%, which is not detectable with our instrumentation. This explains why the purified sample of [Ce^{3+} ⊂ 2.2.1] does not show the quenching.

Since it is well known that Eu^{3+} quenches the Ce^{3+} emission in solids by electron-transfer quenching [19], we replaced 1% of the Ce^{3+} in the purified sample by Eu^{3+}. At 4.2 K, however, there was no appreciable amount of quenching, nor of energy transfer: Ce^{3+} excitation yields Ce^{3+} emission, Eu^{3+} ($4f^6$) excitation yields Eu^{3+} emission. Therefore, it is concluded that a distance of 10 Å is large enough to prevent electron transfer between Ce^{3+} and Eu^{3+} under the present circumstances.

Since the Ce^{3+} emission is situated in the Eu^{3+} charge-transfer absorption region, we calculated the critical distance for energy transfer by dipole–dipole interaction. It appears that $SO = 0.4$ eV^{-1}, $E \simeq 4$ eV and $P = 5 \times 10^{-3}$ (from the experimental values for ϵ and $\Delta_{1/2}$). With these data it follows that R_c = 17 Å. Since charge-transfer excitation of solid [Eu^{3+} ⊂ 2.2.1] does not result in emission [4], this transfer presents a quenching process. In the same way as above, we arrive at an amount of quenching of 12%, hardly detectable under the present experimental conditions. At 300 K the energy migration will result in an increase in the amount of quenching. The sphere determined by the diffusion length will contain 9 Eu^{3+} species (there is 1 Eu^{3+} per 10^5 $Å^3$), so that not every encounter of the excited state with a Eu^{3+} ion results in quenching. This fits with our

calculations. With an R_c value for $Ce^{3+} \rightarrow Ce^{3+}$ transfer of 18 Å and R_c for $Ce^{3+} \rightarrow Eu^{3+}$ transfer of 17 Å, and with 12 neighbours as above, the probability that a Ce^{3+} ion transfers to Eu^{3+} is 1/16 of that for $Ce^{3+} \rightarrow Ce^{3+}$ transfer, assuming only Ce^{3+} ions with one Eu^{3+} neighbour. The probability that the Ce^{3+} excited state is not quenched by the Eu^{3+} ions during the former lifetime is $(15/16)^9 = 56\%$, so that 44% will be quenched. The experimental amount is $1/3 \times 88\% + 12\% = 41\%$. The agreement is much better than expected in view of the approximations made. It cannot be excluded that thermally activated electron transfer also plays a role. In order to decide on this problem, considerably more accurate data are necessary.

The nature of the quenching centres in the impure sample remains unclear. However, since they must be able to perform an effective trapping and be responsible for the tail in the diffuse reflection spectrum, the presence of Ce^{4+} in some form seems an obvious choice.

In conclusion, the solid $[Ce^{3+} \subset 2.2.1]Cl_3$ cryptate shows quenching of its luminescence at room temperature due to energy migration to quenching sites. Due to the large Ce^{3+}–Ce^{3+} distance the total diffusion length is small (60 Å), so that pure samples do not show the quenching. Very similar observations were made for $EuAl_3B_4O_{12}$ [20].

Finally some noteworthy remarks. For (Y, Ce)-$Al_3B_4O_{12}$ [21], with very similar emission and absorption spectra, energy migration over the Ce^{3+} ions was observed with a total number of steps of 420 at 300 K. The shortest Ce–Ce distance here is 5.9 Å. The lower number of steps in the cryptate is due to the larger Ce–Ce distance.

For $[Gd^{3+} \subset 2.2.1]$, no energy migration takes place because 10 Å is too long a distance for the weak interaction forces [22].

No energy transfer is observed for $[Ce^{3+} \subset 2.2.1]$ in solution because the distances are now much larger. No thermal quenching occurs in solution.

No energy transfer is observed for $[Ce^{3+} \subset 2.2.2]$, not even in the solid state at 300 K. This is not surprising; due to the larger Stokes shift and the smaller amount of thermal broadening, the spectral overlap will be considerably smaller. From our spectra we find $SO = 0.02\ eV^{-1}$ and $R_c = 12$ Å, so that transfer has only a small probability (especially since the Ce^{3+}–Ce^{3+} distance will also be larger than 10 Å).

Within the family of rare earth cryptates the case of energy migration in $[Ce^{3+} \subset 2.2.1]$ is, therefore, unique.

Comparison with Eu^{2+} Cryptates

The $[Eu^{2+} \subset 2.2.1]$ and $[Eu^{2+} \subset 2.2.2]$ cryptates have been studied in solution [2]. At room temperature they show only very weak luminescence (quantum efficiency 10^{-3}), but at low temperatures the efficiencies become 1. The $[Eu^{2+} \subset 2.2.1]$ species shows a Stokes shift of about 8000 cm^{-1} and that of the $[Eu^{2+} \subset 2.2.2]$ complex 9700 cm^{-1}. Since the relevant transitions are also of the $f \rightarrow d$ type, a comparison with the present results on Ce^{3+} cryptates in solution is feasible.

The values of the Stokes shifts are larger for Eu^{2+}. Furthermore, the absorption transitions in the case of Eu^{2+} are at slightly lower energy than those of Ce^{3+}, *viz.* some 2000 cm^{-1}. The latter effect may contribute to a lower quenching temperature of the luminescence [23], but is not expected to be responsible for the total, rather large difference. It must be the larger Stokes shift which causes the lower quenching temperature in the case of Eu^{2+} [23].

Relative to the Ce^{3+} ion, the Eu^{2+} ion carries an effectively negative charge. It has been argued elsewhere that this will result in larger parabolae offset in the configurational coordinate diagram, *i.e.* larger Stokes shift. In this connection it is interesting to compare the results for Eu^{2+} in $EuAlO_3$, which also carries an effectively negative charge [24]. Its luminescence characteristics are very similar to those for $[Eu^{2+} \subset 2.2.1]$ with a value of the Stokes shift of 8000 cm^{-1} and a quenching temperature below 300 K.

Since the Eu^{2+} ion has an ionic radius which is 0.1 Å larger than the Ce^{3+} ion [13], and the Ce^{3+} ion fits exactly in the [2.2.1] cavity, the large difference between the Stokes shifts of $[Ce^{3+} \subset 2.2.1]$ and $[Eu^{2+} \subset 2.2.1]$ probably has yet another reason, *viz.* another configuration. For the [2.2.1] cryptates there are two possible configurations: **A**, in which each of the three holes in the cryptand cage is occupied by a water molecule from the aqueous solution [3], and **B**, in which only the larger one of the three holes in the cryptand cage (defined by the two strands containing two oxygen atoms) is used for coordination, in addition to the cryptand itself [25]. The latter one has been observed in an X-ray diffraction study on $[Ln \subset 2.2.1](ClO_4)_3 \cdot 2CH_3CN$ ($Ln = Pr^{3+}$ or Er^{3+}) [25].

Since the Ce^{3+} ion feels a strong constraint (see above), $[Ce^{3+} \subset 2.2.1]$ is expected to have the **A** configuration. However, the larger Eu^{2+} ion will probably not fit into this configuration and we may expect $[Eu^{2+} \subset 2.2.1]$ to have the **B** configuration. This offers a weaker constraint which will result in a larger Stokes shift. If Ce^{3+} fits exactly, the Eu^{3+} ion (0.07 Å smaller [13]) does not fit and could prefer the **B** configuration. The structural information obtained from the emission in the presence of F^- does not exclude that configuration [26]. The Eu^{2+} ion is still too small to fit into the [2.2.2] cavity, so that it is expected to show a certain off-centre position like the Ce^{3+} ion.

Finally, we note that the Eu^{2+} ion can also form a complex with 18-crown-6-ethers [27]. The Eu^{2+} ion

TABLE II. Cubic Crystal-field Splitting (Δ) for Several Complexes in Solution as Derived from Absorption and/or Excitation Spectra

Complex	Δ (10^3 cm^{-1})	Reference
[Ce^{3+} ⊂ 2.2.2], aqueous solution	7	This work
[Eu^{2+} ⊂ 2.2.2], aqueous solution	8	2
Eu^{2+}·18-crown-6, methanolic solution	8	27
Yb^{2+}·18-crown-6, methanolic solution	7	30
Ce^{3+} in $Y_3Al_5O_{12}$, solid state	14	7
Eu^{2+} in SrF_2, solid state	15.6	31

TABLE III. Crystal-Field Components and their Differences of the 5d Level of Ce^{3+} and Eu^{2+} in the [2.2.1] Cryptand and of the $^7F_2$ Level of [Eu^{3+} ⊂ 2.2.1] (All values are in 10^3 cm^{-1})

Complex					
[Ce^{3+} ⊂ 2.2.1] aqueous solution [this work]		[Eu^{2+} ⊂ 2.2.1] aqueous solution [2]		[Eu^{3+} ⊂ 2.2.1] solid state [4]	
33.3	5.0	27.2	3.2	16.115	0.028
38.3	5.2	30.4	3.7	16.143	0.058
43.5	2.0	34.1	2.5	16.201	0.036
45.5	3.5	36.6	2.8	16.237	0.034
49.0		39.4		16.271	

is accommodated in the cavity of the crown. This complex emits at 300 K (quantum efficiency 0.09) with a Stokes shift of 8000 cm^{-1}. This has been discussed more in detail in ref. 19.

Crystal-field Splitting of the Excited 5d Level

The crystal-field splitting of the excited 5d level of ions with excited $4f^{n-1}5d$ states can be derived from the absorption and/or excitation spectra [7, 28]. For $Ce^{3+}(4f^1)$ this is straight forward; for Eu^{2+} ($4f^7$) the exchange interaction between the $4f^6$ and the 5d electrons must be strong [29], but in the present complexes with a low degree of covalency (see above) this is most probably fulfilled. In Table II we have collected some data on [2.2.2] cryptates and 18-crown-6 complexes. These have D_{3d} site symmetry for the rare earth ion in good approximation which makes it possible to derive the cubic crystal-field splitting (Δ). For comparison, values are added for solids in which the rare earth ion has a cubic eight-coordination.

It is immediately clear that the crystal-field splitting in the cage-type complexes is about half that in solids; a difference which was also observed for Eu^{3+} [4]. The value for Yb^{2+} ($4f^6$) was recalculated from data in ref. 30. In that paper a Stokes shift of 1700 cm^{-1} was given for the very weak 5d → 4f emission of Yb^{2+} in 18-crown-6. In view of the values for Stokes shifts reported above, it seems realistic to consider this emission as emission from a higher excited state. This point needs further study.

For the [2.2.1] cryptates the situation is more complicated, since the coordination involved does not bear any resemblance to a cube. Table III compares the 5d components for the Ce^{3+}, Eu^{2+} and Eu^{3+} [2.2.1] cryptates. Note that the data for Eu^{3+} refer to the $^7F_2$ splitting [4]. This level is also five-fold degenerate, as is the 5d level. The overall splittings in the case of Ce^{3+} and Eu^{2+} are not very different from those in the [2.2.2] cryptates. The $^7F_2$ splitting is, of course, two orders of magnitude smaller. The splitting pattern for Ce^{3+} and Eu^{2+} is different: if we go from the lowest to the highest crystal-field component, Ce^{3+} shows two large and two smaller splittings, but Eu^{2+} shows four splittings which are not markedly different if we take account of the experimental errors. This difference in splitting pattern may correspond to a different configuration of the cryptate, as suggested above. We conclude, therefore, that [Ce^{3+} ⊂ 2.2.1] has the A configuration because of the excellent fit of the Ce^{3+} ion in the cavity, whereas [Eu^{2+} ⊂ 2.2.1] and [Eu^{3+} ⊂ 2.2.1] have the B configuration because the ionic radii of the central ions are too large or too small, respectively, to fit the [2.2.1] cavity.

Acknowledgements

G.B. and N.S. acknowledge a travel grant within the framework of cooperation between the Universities of Bologna and Utrecht. N.S. and S.P. acknowledge financial support from the Ministero della Pubblica Istruzione.

References

1 J. M. Lehn, *Acc. Chem. Res., 11*, 49 (1978).
2 N. Sabbatini, M. Ciano, S. Dellonte, A. Bonazzi, F. Bolletta and V. Balzani, *J. Phys. Chem., 88*, 1534 (1984).
3 N. Sabbatini, S. Dellonte, M. Ciano, A. Bonazzi and V. Balzani, *Chem. Phys. Lett., 107*, 212 (1984).
4 G. Blasse, M. Buijs and N. Sabbatini, *Chem. Phys. Lett., 124*, 538 (1986).
5 N. Sabbatini, S. Dellonte and G. Blasse, *Chem. Phys. Lett., 129*, 541 (1986).
6 G. Blasse and N. Sabbatini, *J. Solid State Chem.*, in press.
7 G. Blasse and A. Bril, *J. Chem. Phys., 47*, 5139 (1967).
8 D. Curie, in B. Di Bartolo (ed.), 'Optical Properties of Ions in Solids', Plenum, New York, 1975, p. 78.
9 F. A. Kröger and J. Bakker, *Physica, 8*, 628 (1941).
10 S. W. S. McKeever, M. D. Brown, R. J. Abbundi, H. Chan and V. K. Mathur, *J. Appl. Phys., 60*, 2505 (1986).
11 E. Loh, *Phys. Rev., 154*, 270 (1967).
12 A. G. Svetashev and M. P. Tsvirko, *Opt. Spectrosc. (USSR), 56*, 515 (1984).
13 R. D. Shannon, *Acta Crystallogr., Sect. A, 32*, 751 (1976).
14 W. T. Carnall, in K. A. Gschneider Jr. and L. Eyring (eds.), 'Handbook on the Physics and Chemistry of Rare Earths', North Holland, Amsterdam, 1979, Chap. 24.
15 D. L. Dexter, *J. Chem. Phys., 21*, 836 (1953).
16 G. Blasse, *Philips Res. Rep., 24*, 131 (1969).
17 E. L. Yee, J. T. Hupp and M. J. Weaver, *Inorg. Chem., 22*, 3465 (1983).
18 G. Kortüm, 'Reflectance Spectroscopy', Springer Verlag, Berlin, 1969.
19 G. Blasse and N. Sabbatini, *Mat. Chem. Phys., 16*, 237 (1987); G. Blasse, *Phys. Status Solidi A, 75*, K41 (1983); G. Blasse, *Chem. Phys. Lett., 56*, 409 (1978).
20 F. Kellendonk and G. Blasse, *J. Chem. Phys., 75*, 561 (1981).
21 F. Kellendonk, T. van den Belt and G. Blasse, *J. Chem. Phys., 76*, 1194 (1982).
22 A. J. de Vries, H. S. Kiliaan and G. Blasse, *J. Solid State Chem., 65*, 190 (1986).
23 G. Blasse, *J. Chem. Phys., 51*, 3529 (1969); K. C. Bleijenberg and G. Blasse, *J. Solid State Chem., 28*, 303 (1979); G. Blasse, *J. Solid State Chem., 9*, 147 (1974).
24 P. M. Jaffe, *J. Electrochem. Soc., 117*, 918 (1970).
25 J. F. Desreux, P. P. Barthelemy, M. R. Spirlet and J. J. Rebizant, *J. Less-Common Met., 126*, 400 (1986).
26 N. Sabbatini, S. Perathoner, G. Lattanzi, S. Dellonte and V. Balzani, *J. Phys. Chem.*, in press.
27 G. Y. Adachi, K. Sorita, K. Kawata, K. Tomokiyo and J. Shiokawa, *Inorg. Chim. Acta, 109*, 117 (1985).
28 G. Blasse, W. L. Wanmaker, J. W. ter Vrugt and A. Bril, *Philips Res. Rep., 23*, 189 (1968).
29 F. M. Ryan, W. Lehmann, D. W. Feldman and J. Murphy, *J. Electrochem. Soc., 121*, 1475 (1974).
30 Wenlian Li, H. Fujikawa, G. Y. Adachi and J. Shiokawa, *Inorg. Chim. Acta, 117*, 87 (1986).
31 A. A. Kaplyanskii and P. P. Feofilov, *Opt. Spectrosc. (USSR), 13*, 129 (1962).